ความแม่นของการวัดเชิงเส้นระหว่างการใช้โปรแกรมการเย็บกับไม่ใช้ในภาพรังสีส่วนตัดอาศัยคอมพิวเตอร์แบบลำรังสีรูปกรวย

นางสาวปรียพร ศรีมาวงษ์

วิทยานิพนธ์นี้เป็นส่วนหนึ่งของการศึกษาตามหลักสูตรปริญญาวิทยาศาสตรมหาบัณฑิต

สาขาวิชาฉายาเวชศาสตร์ ภาควิชารังสีวิทยา

คณะแพทยศาสตร์ จุฬาลงกรณ์มหาวิทยาลัย

ปีการศึกษา 2554

ACCURACY OF LINEAR MEASUREMENTS IN STITCHED VERSUS NON-STITCHED CONE BEAM COMPUTED TOMOGRAPHY IMAGES

Miss Preeyaporn Srimawong

A Thesis Submitted in Partial Fulfillment of the Requirements
for the Degree of Master of Science Program in Medical Imaging

Department of Radiology
Faculty of Medicine
Chulalongkorn University

Academic Year 2011

Thesis Title	ACCURACY OF LINEAR MEASUREMENTS IN STITCHED VERSUS NON-STITCHED CONE BEAM COMPUTED TOMOGRAPHY IMAGES
By	Miss Preeyaporn Srimawong
Field of Study	Medical Imaging
Thesis Advisor	Associate Professor Anchali Krisanachinda, Ph.D.
Thesis Co-advisor	Jira Chindasombatjaroen, Ph.D.

Accepted by the Faculty of Medicine, ChulalongkornUniversity in Partial Fulfillment of the Requirements for the Master's Degree

....Dean of the Faculty of Medicine
(Associate Professor Sophon Napathorn, M.D.)

THESIS COMMITTEE

.... Chairman
(Associate Professor Sukalaya Lerdlum, M.D.)

....Thesis Advisor
(Associate Professor Anchali Krisanachinda, Ph.D.)

....Thesis Co-advisor
(Jira Chindasombatjaroen, Ph.D.)

.... External Examiner
(Professor Franco Milano, Ph.D.)

ปรียพร ศรีมาวงษ์: ความแม่นของการวัดเชิงเส้นระหว่างการใช้โปรแกรมการเย็บกับไม่ใช้ในภาพรังสีส่วนตัดอาศัยคอมพิวเตอร์แบบลำรังสีรูปกรวย.(ACCURACY OF LINEAR MEASUREMENTS IN STITCHED VERSUS NON-STITCHED CONE BEAM COMPUTED TOMOGRAPHY IMAGES) อ.ที่ปรึกษาวิทยานิพนธ์หลัก: รศ.ดร.อัญชลี กฤษณจินดา, อ. ที่ปรึกษาวิทยานิพนธ์ร่วม: อ.ทญ.ดร.จิรา จินดาสมบัติเจริญ, 55 หน้า.

การนำภาพรังสีส่วนตัดอาศัยคอมพิวเตอร์แบบลำรังสีรูปกรวยมาใช้นั้น การวัดเชิงเส้น เป็นสิ่งจำเป็นที่จะช่วยให้การวางแผนการรักษามีความแม่นยำมากขึ้น ดังนั้น ความแม่นของการวัดเชิงเส้นในภาพรังสีนี้ จึงเป็นสิ่งที่สำคัญอย่างยิ่งที่ควรตรวจสอบยืนยัน ปัจจุบันมีโปรแกรมเรียกว่า stitching program หรือโปรแกรมการเย็บ ในเครื่องรุ่น Kodak 9000C 3D ซึ่งสามารถเชื่อมตำแหน่งขนาดของบริเวณที่ถ่ายเล็ก ๆ 3 ขนาด ให้มีขนาดใหญ่ขึ้น โดยที่ขนาด voxel เล็ก ทำให้ได้ภาพบริเวณกว้างขึ้น แต่มี resolution ที่ดีกว่าภาพรังสีที่ถ่ายจากเครื่องที่มีขนาดของบริเวณที่ถ่ายใหญ่ วัตถุประสงค์ของการศึกษานี้ คือ เพื่อประเมินความแม่นของการวัดเชิงเส้นระหว่างการใช้โปรแกรมการเย็บกับไม่ใช้ในภาพรังสีส่วนตัดอาศัยคอมพิวเตอร์แบบลำรังสีรูปกรวยเมื่อเปรียบเทียบกับการวัดโดยตรง

การศึกษานี้ทำในกระดูกขากรรไกรล่างจำนวน 10 ชิ้น โดยกำหนดจุดที่กระดูกตามตำแหน่งอ้างอิง โดยใช้วัสดุอุดคลองรากฟัน จะได้ระยะในแนวตั้งและแนวนอนทั้งหมด 10 ระยะ ใช้ digital caliper วัดโดยตรงที่กระดูก ซึ่งเป็น gold standard การวัดในแต่ละระยะจะวัด 3 ครั้ง คนละวันกัน แล้วหาค่าเฉลี่ย นำกระดูกขากรรไกรไปถ่ายภาพรังสีส่วนตัดอาศัยคอมพิวเตอร์แบบลำรังสีรูปกรวย โดยใช้โปรแกรมการเย็บกับไม่ใช้โปรแกรมการเย็บ แล้ววัดระยะเดียวกันในภาพรังสี แต่ละระยะจะวัด 3 ครั้ง คนละวันกัน แล้วหาค่าเฉลี่ย จากนั้นจึงวิเคราะห์ผลที่ได้จากการวัด

ผลที่ได้จากการวิจัย คือ การวัดตรงมีค่า intraclass correlation coefficients เป็น 0.998 ถึง 1.00 การวัดในภาพรังสีโดยใช้โปรแกรมการเย็บกับไม่ใช้มีค่า intraclass correlation coefficients เท่ากับ 1.000 แสดงถึงการวัดที่มีความแม่นยำอย่างมากในผู้วัดคนเดียวกัน เมื่อเปรียบเทียบการวัดโดยตรงกับการวัดในภาพรังสีโดยไม่ใช้โปรแกรมการเย็บ พบว่า ค่า intraclass correlation coefficients เท่ากับ 0.972 ถึง 1.000 และเมื่อเปรียบเทียบการวัดโดยตรงกับการวัดในภาพรังสีโดยใช้โปรแกรมการเย็บ พบว่า ค่า intraclass correlation coefficients เท่ากับ 0.967 ถึง 0.998

สรุปผลที่ได้จากการวิจัยนี้ คือ ไม่มีความแตกต่างกันอย่างมีนัยสำคัญทางสถิติระหว่างการวัดโดยตรงและการวัดในภาพรังสีส่วนตัดอาศัยคอมพิวเตอร์แบบลำรังสีรูปกรวย โดยใช้โปรแกรมการเย็บกับไม่ใช้ ($P > 0.05$)

ภาควิชา	รังสีวิทยา	ลายมือชื่อนิสิต ปรียพร ศรี
สาขาวิชา	ฉายาเวชศาสตร์	ลายมือชื่อ อ.ที่ปรึกษาวิทยานิพนธ์หลัก
ปีการศึกษา	2554	ลายมือชื่อ อ.ที่ปรึกษาวิทยานิพนธ์ร่วม

#5374645730: MEDICAL IMAGING
KEYWORDS: CBCT / KODAK 9000C 3D / ACCURACY / STITCHING PROGRAM

PREEYAPORN SRIMAWONG: ACCURACY OF LINEAR MEASUREMENTS IN STITCHED VERSUS NON-STITCHED CONE BEAM COMPUTED TOMOGRAPHY IMAGES. THESIS ADVISOR: ASSOC.PROF.ANCHALI KRISANACHINDA, THESIS CO-ADVISOR: JIRA CHINDASOMBATJAROEN, 55 pp.

Cone beam computed tomography (CBCT) images are useful in clinical dentistry. Linear measurements are necessary for accurate treatment planning. Current program called stitching program in Kodak 9000C 3D systems automatically combines up to three localized volumes to construct larger images with small voxel size. The purpose of this study was to assess the accuracy of linear measurements from stitched and non-stitched CBCT images in comparison to direct measurements.

This study was performed in 10 human dry mandibles. Gutta-percha rods were marked at reference points to obtain 10 vertical and horizontal distances. Direct measurements by digital caliper were served as gold standard. All distances on CBCT images obtained by using and not using stitching program were measured, and compared with direct measurements. The intraclass correlation coefficients (ICCs) were calculated.

The ICCs of direct measurements were 0.998 to 1.000. The ICCs of intra-observer of both non-stitched CBCT images and stitched CBCT images were 1.000 indicated strong agreement made by a single observer. The inter-method ICCs between direct measurements vs non-stitched CBCT images and direct measurements vs stitched CBCT images ranged from 0.972 to 1.000 and 0.967 to 0.998, respectively. No statistically significant differences between direct measurements and stitched CBCT images or non-stitched CBCT images ($P > 0.05$).

Department : Radiology	Student's Signature Preeyaporn Srimawong
Field of Study : Medical Imaging	Advisor's Signature Anchali K.
Academic Year : 2011	Co-advisor's Signature

ACKNOWLEDGEMENTS

I would like to express gratitude and deepest appreciate to Associate Professor Anchali Krisanachinda, Ph.D., and Lecturer Jira Chindasombatjaroen, Ph.D., my major advisor and co-advisor for their guidance, invaluable advice, supervision, constructive comments and English language proof in this research.

I would like to thank Associate Professor Sukalaya Lerdlum, M.D., who was the chairman of thesis defence and Professor Franco Milano, Ph.D., who was the external examiner for their kind suggestion and constructive comments in this research.

I would like to thank Associate Professor Sivalee Suriyapee, M.Eng. for teaching of knowledge in Medical Imaging and comments in this research.

I would like to thank Associate Professor Jantima Roongruangchai, Ph.D., for her kindness to lend mandibles, Assistant Professor Somchai Chairoongruang, M.D., Associate Professor Pipat Chiewvit, M.D., and Mrs.Wandee Planuphap, D.D.S. for their permission to use cone beam computed tomography machine at Faculty of Medicine Siriraj Hospital.

I would like to thank Lecturer Tawepong Arayapisit, Assistant Professor Roongrawee Kamolroongwarakul, and Mr.Paradon Pateetin for their kindness to give materials using in this research.

I would like to thank Mrs.Petcharleeya Suwanpradit, Ms.Walaiporn Khuenkaew, Mr.Kittiwat Khamwan, Mr.Pairat Munee, Mr.Thitirat Jamjan and Mrs.Natchaya Amornmettajit for their help.

I would like to thank Mr.Wasan Panyasang and Mrs.Weeranuch Kitsukjit who were consultant in statistical analysis.

I would like to thank all teachers, lecturers and staff in Master of Science Program for their unlimited teaching of knowledge in Medical Imaging.

I would like to thank Assistant Professor Suchaya Pornprasertsuk-Damrongsri and lecturers in Department of Oral and Maxillofacial Radiology, Faculty of Dentistry, Mahidol University for their support and sympathies.

Finally, I would like to deepest thank Mr.Tawan Wannarat and my family. They always encourage, take care, financial support and understand me. That’s valuable for me.

CONTENTS

Page

LIST OF TABLES

Table **Page**

LIST OF FIGURES

LIST OF ABBREVIATIONS

ABBREVIATION	TERMS
2D	Two-dimension
3D	Three-dimension
3M	Minnesta Mining and Manufacturing
μSv	Microsieverts
a-Si	Amorphous silicon
CBCT	Cone beam computed tomography
CBVI	Cone beam volumetric imaging
CBVT	Cone beam volumetric tomography
CCD	Charge coupled device
cm	Centimeter
CMOS	Complementary metal-oxide semiconductor
Co	Company
Corp	Corporation
CsI	Cesium iodide
CT	Computed tomography
e.g	Exempli gratia, for example
et al	Et alibi, and others
FBP	Filtered back projection
FOV	Field of view
FPD	Flat panel detector
HU	Hounsfield units

ABBREVIATION	**TERMS**
HVL	Half-value layer
ICCs	Intraclass correlation coefficients
ICRP	International Commission on Radiological Protection
II	Image intensifier
Inc	Incorporation
Ltd	Limited
MDCT	Multidetector computed tomography
MIP	Maximum intensity projection
mm	Millimeter
mm^3	Cubic millimeter
Mfg	Manufacturing
MPR	Multiplanar reformation
no	Number
r	Pearson correlation coefficient
ROI	Region of interest
SIRB	Siriraj Institutional Review Board
SPSS	Statistical Package for Social Science
TFT	Thin film transistor
USA	United States of America

CHAPTER I

INTRODUCTION

1.1 Background and Rationale

Cone beam computed tomography (CBCT) has been given several names including cone beam volumetric tomography (CBVT), cone beam volumetric imaging (CBVI), dental volumetric tomography, dental computed tomography, digital volume tomography and cone beam imaging. The most preferred term is cone beam computed tomography.[1] The CBCT technique has been used initially for fluoroscopic systems in 1976,[2] radiotherapy in 1978[3, 4] and angiography in 1982.[5] The CBCT technique has also been used in microtomography of small specimens for biomedical and industrial applications.[6]

CBCT is an advanced technique that demonstrates the interested tissue in three dimensions. Early CBCT scanners for dental use were developed by Mozzo et al.[7] and Arai et al.[8] in late 1990s. Nowadays CBCT has become an important imaging method for diagnosis, treatment planning and evaluation of treatment outcomes. The basic principle of CBCT is a cone-shaped x-ray beam and detector rotation around the patient's head. There are different types of detectors including amorphous silicon (a-Si), cesium iodide (CsI), complementary metal-oxide semiconductor (CMOS), flat panel detector (FPD) or charge coupled device (CCD) with image intensifier (II). After the beam passes through patient, the remnant beam is captured on an area detector. Then, the scanning software collects the raw image data and reconstructs into viewable formats resulting in the production of a digital volume.

CBCT scanner uses cone shaped x-ray beam rather than a conventional fan beam, as in medical Computed Tomography (CT), to provide images of the bony structures of the skull. As a result, the medical CT scanner provides a set of consecutive slices of the patient while the CBCT scanner provides a volume of data. During a CBCT scan, the scanner rotates around the patient's head, a detector captures the remnant beam and the scanning software reconstructs the data into images, producing a digital volume composed of three dimensional blocks of small cuboid structures. The smallest subunit of a digital volume is called a voxel or volume element. Each voxel is assigned a gray-scale value and characterized with the same height, width and depth. CBCT images can be visualized as 2D multiplanar reformatted slices or in 3D by using surface reconstruction or volume rendering.

CBCT systems offer many benefits beyond multidetector computed tomography (MDCT) for dental treatment and planning, including lower radiation dose,[9, 10] lower costs,[11] smaller apparatus[11] and easier operation. On the other hand, the limitations of CBCT are dynamic range of x-ray detectors resulting in lack of soft tissue discrimination,[8] the ability to adjust collimation or exposure parameters on some units, more image noise than MDCT and inability to express actual Hounsfield units (HU) as available in MDCT.

CBCT images are useful in clinical dentistry including treatment planning for dental implants, demonstrating the impacted tooth and its adjacent vital structures, evaluating dental and osseous disease in the jaws, evaluating growth and development for orthodontics, imaging for management of endodontic problems and evaluating of craniofacial fractures. Linear measurements are necessary for accurate treatment planning in dental implant surgery for the alveolar bone height and width measurements and in oral diagnosis for measurements of dimension of lesions. Therefore, the accuracy of linear measurements on CBCT images is needed to be verified.

Currently, there are 2 types of CBCT systems according to the size of field of view (FOV).

1) Limited or Regional CBCT

The size of FOV varies from 4 - 10 cm in diameter and height. The voxel sizes can be as small as 0.07 - 0.20 mm^3.

2) Full or Facial CBCT

The size of FOV varies from 11 - 24 cm in diameter and height. The voxel size ranges from 0.25 - 0.40 mm^3.

It should be noted that larger FOV resulting in the larger voxel size and therefore, lower resolution images.

There are currently optional program called stitching program in few CBCT machines e.g. Kodak 9000 3D (Carestream Health, Inc., New York, USA) systems. This program automatically combines up to three localized volumes to construct larger images with voxel size 0.20 mm^3. To use the program, the stitching option is selected during acquisition setup. After all exposures, the software automatically combines the acquired volumes and reconstruction to create one large image. However, the accuracy of linear measurements in stitching CBCT images has not been reported.

1.2 Hypothesis

1.2.1 Null Hypothesis (H_0): There are no differences in the linear measurements on stitched and non-stitched CBCT images in comparison to the direct measurements.

1.2.2 Alternative Hypothesis (H_1): There are differences in the linear measurements on stitched and non-stitched CBCT images in comparison to the direct measurements.

1.3 Objective

To assess the accuracy of linear measurements from stitched and non-stitched CBCT images in comparison to direct measurements

CHAPTER II

REVIEW OF RELATED LITERATURES

2.1 Theory

2.1.1 Basic principle of Cone Beam Computed Tomography[1]

Cone beam CT scanner consists of an x-ray source and detector (Figure 2.1). During rotation of the gantry, the receptor detects x-ray attenuated by the patient. These recordings constitute "raw data" that is reconstructed by a computer algorithm to generate cross-sectional images with component picture element (pixel) values.

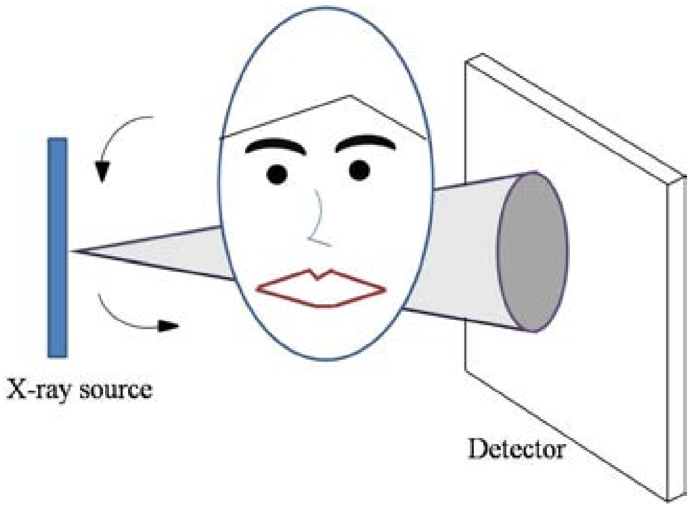

Figure 2.1 Cone shaped x-ray beam in CBCT.

Cone beam CT scanners use a two-dimensional digital array providing an area detector rather than a linear detector as medical CT does. Only one rotational scan of the gantry is necessary to acquire enough data for image reconstruction. CBCT produces an entire volumetric dataset from which the voxels are extracted. Voxel dimensions are dependent on the pixel size on the area detector. Therefore CBCT units in general provide voxel resolutions that are isotropic in all 3 dimensions. In medical CT, the voxels are anisotropic which the longest dimension is the axial slice thickness and determined by slice pitch.

2.1.2 Image acquisition[1]

The CBCT technique requires only a rotational scan. A reciprocating area detector moves synchronously around the patient's head. During the rotation, many exposures are made at fixed intervals, providing single projection images known as basis images. The complete series of basis images is referred to as the projection data. Software programs including filtered back projection (FBP) are applied to these projection data to generate a 3D volumetric data set that can be used to provide primary reconstruction images in three orthogonal planes (axial, sagittal and coronal).

There are four components to CBCT image acquisition:

2.1.2.1 CBCT system design

2.1.2.2 Image detection system

2.1.2.3 Image reconstruction

2.1.2.4 Image display

2.1.2.1 CBCT system design

CBCT can be performed with the patient in three positions including sitting, standing and supine. The scan times are often greater than that used with panoramic imaging, perhaps more important than patient orientation is the head restraint mechanism used. With all machines it is important to immobilize the patient's head because any movement degrades the final image.

During the rotation, each projection image is made by sequential single-image capture of the remnant x-ray beam by the detector. The methods of exposing the patient can be divided into two groups. The first one is continuous radiation exposure to the patient during the rotation. Another one is pulse x-ray beam to coincide with the detector sampling. This means that actual exposure time is markedly less than scanning time. This technique reduces patient radiation dose considerably.

The dimensions of the field of view or scan volume able to be covered are primarily dependent on the detector size and shape, beam projection geometry and the ability to collimate the beam. The shape of the scan volume can be either a cylinder or sphere. Collimating the primary x-ray beam limits x-radiation exposure the region of interest (ROI). Limiting field size therefore ensures that an optimal field of view can be selected for each patient on the basis of individual needs. Scanning of the whole craniofacial region is difficult to incorporate into cone beam design because the cost of large area detectors is high.

The speed which individual images are acquired is called the frame rate. Higher frame rates increase primary reconstruction time and signal to noise ratio, producing images with less noise. In the maxillofacial region, another advantage of a higher frame rate is that it reduces metallic artifact. However, higher frame rates are usually accomplished with a longer scan time and higher patient dose.

2.1.2.2 Image detection system

There are two types of image detection: image intensifier tube/charge-coupled device combination and flat panel detector. The former consists of an x-ray image intensifier tube coupled to a charge coupled device with a fiber optic coupling. The latter comprises detection of x-rays with an indirect detector that is based on a large area solid state sensor panel coupled to an x-ray scintillator layer. The most common flat panel detector consists of a cesium iodide scintillator applied to a thin film transistor (TFT) made of amorphous silicon. CsI scintillator produces superior spatial resolution because of the microscopic columnar structure of the CsI substrate which serves essentially as a fiber-optic conductor for the signal intensity being transmitted to the photodiode array.[12] FPD arrays can afford greater spatial resolving potential with similar noise intensity when compared with II tube/CCD.[13]

2.1.2.3 Image reconstruction

Once the basis projection frames have been acquired, it is necessary to process these data to create the volumetric data set. This process is called primary reconstruction. The reconstruction of these data is computationally complex. To facilitate data handling, data are usually acquired by one computer (acquisition computer) and transferred by an Ethernet connection to a processing computer (workstation). In contrast to conventional CT, cone beam data reconstruction is performed by personal computer based rather than workstation platforms.

Reconstruction times vary depending on the acquisition parameters (voxel size, size of the image field and number of projections), hardware (processing speed, data throughput from acquisition to workstation computer) and software (reconstruction algorithms) used. Reconstruction should be accomplished in an acceptable time to complement patient flow.

The process as illustrated in figure 2.2 consists of two stages.

2.1.2.3.1 Acquisition stage

This stage is done at the acquisition computer. Once the multiple planar projection images are acquired, these images must be corrected by for inherent pixel imperfections and uneven exposure. Image calibration should be performed regularly to remove these defects.

The acquisition stage involves acquisition of individual basis projections and subsequent modification of these images to correct for inconsistencies. Image correction is sequential and consists of the removal of signal voids from individual or linear pixel defects, image normalization by histogram equalization so that a full range of voxel intensity values are used and removal of inherent electronic detector artifacts.

2.1.2.3.2. Reconstruction stage

The remaining data are done at the reconstruction computer. The corrected images are converted into a special representation called a sinogram, a composite image developed from extracting a row of pixels from each projection image. Therefore the first sinogram will comprise a series of the first rows from each projection. This process is referred to as the radon transformation. The resulting image comprises multiple sine waves of different amplitude. The sinogram is then reconstructed with a filtered back-projection algorithm for CBCT-acquired volumetric data called the Feldkamp algorithm. Once all slices have been reconstructed, they are combined into a single volume for visualization.

The reconstruction stage includes converting the corrected basis projection images into sinograms and application of the Feldkamp reconstruction to the corrected sonograms which includes weighting the information according to location, applying specific filters to the image and finally use of back-projection techniques to reconstitute the image.

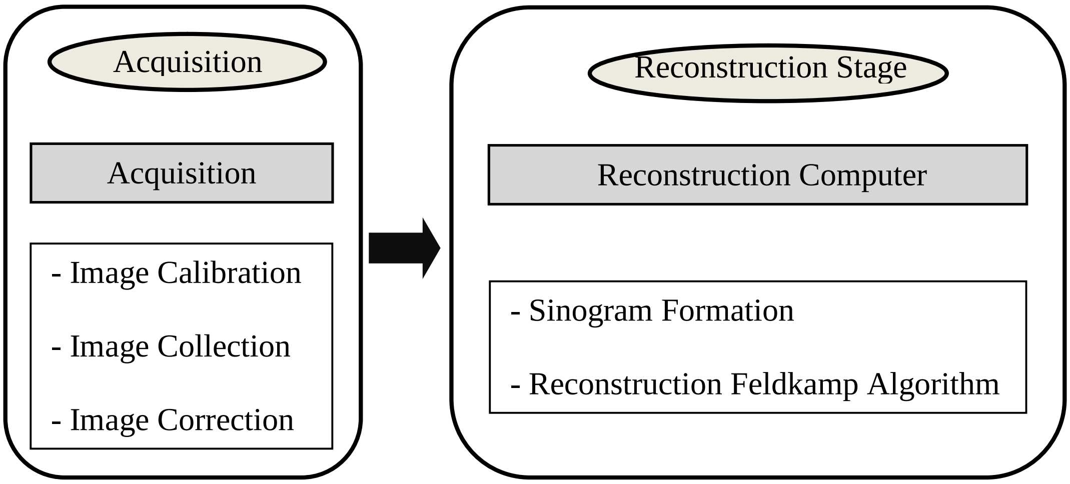

Figure 2.2 Image acquisition and reconstruction in CBCT

2.1.2.4 Image display

The volumetric data set is a compilation of all voxels and, most CBCT devices, is presented on screen as secondary reconstructed images in three orthogonal planes (axial, sagittal and coronal), usually at a thickness defaulted to the native resolution. Optimum visualization of orthogonal reconstructed images is dependent on the adjustment of window level and window width to bone and the application of specific filters.

Most software provides various nonaxial two-dimensional images, referred to multiplanar reformation (MPR). MPR modes contain oblique, curved planar reformation and serial transplanar reformation. Any multiplanar image can be thickened by increasing the number of adjacent voxels included in the display. This creates an image slice that represents a specific volume of the patient referred to as a ray sum. Full-thickness perpendicular ray sum images can be used to produce simulated projections such as lateral cephalometric images. These ray sum images are without magnification and parallax distortion different from conventional radiographs. Nevertheless, this technique uses the total of volumetric data set and occurs more anatomic noise – the superimposition of multiple structures.

Three-dimensional volume rendering refers to techniques which permit the visualization of 3D data by integration of large volumes of nearby voxels and selective display. There are two specific techniques including indirect and direct volume rendering. Indirect volume rendering is a complicated process requiring selection of the intensity or density of the grayscale level of the voxels to be displayed within an entire data set called segmentation. Manual segmentation is often accomplished by an adjustable scale determining the upper and lower limit and range of intensity values. This is technically demanding and computationally difficult requiring specific software. However, it provides a volumetric surface reconstruction with depth. Direct volume rendering is not complicated process. The most common technique is maximum intensity projection (MIP). MIP visualizations are received by evaluating each voxel value along an imaginary projection ray from the viewer's eyes within a particular volume of interest and representing only the highest value as the display value. Voxel intensities that are below an arbitrary threshold are eliminated.

2.1.3 Strengths and Weakness[1]

Cone beam imaging has a number of characteristics suitable for dental applications. However, it also has a number of limitations.

2.1.3.1 Strengths:

A) Size and Cost

CBCT system has a greatly reduced size compared with conventional CT. The cost is approximately one fourth to one fifth of conventional CT. These make it available for the dental clinic.

B) High-speed scanning

The scanning time of CBCT is considerably reduced. It is less than 30 seconds because the CBCT requires only a single scan to capture the necessary data whereas several fan beam rotations in conventional CT scanners are required to complete the imaging of an object.

C) Sub millimeter resolution

All CBCT units currently use megapixel solid-state devices for x-ray detection. These devices provide sub millimeter pixel resolution of component basis projection images. The voxel size determines the image resolution. CBCT makes images with voxel resolution ranging from 0.076 mm to 0.40 mm.[1] This characteristic produces the same resolution of coronal and MPR of CBCT data as axial data. This level of spatial resolution is applicable for maxillofacial applications.

D) Low patient radiation dose

Publication research reports the effective dose based on the International Commission on Radiological Protection (ICRP) 2005 recommendations for various CBCT machines ranges from 52 to 1025 microsieverts (µSv)[1] depending on the type and model of CBCT devices and imaging protocol. These values are approximately equivalent to 4 to 77 digital panoramic radiographs (approximately 13.3 µSv).[1] CBCT provides a range dose reductions between 51% and 96% compared with conventional head CT (1.4to 2.1 mSv).[1]

E) Interactive analysis

CBCT data reconstruction and viewing can be performed by personal computer. Besides, some manufacturers provide software for specific applications such as implant planning or orthodontic analysis.

2.1.3.2 Weakness:

The weakness of the CBCT related to the cone beam projection geometry, detector sensitivity and contrast resolution are:

A) Image noise

The acquisition geometry of cone beam projection results a large volume irradiated with every basis image projection. A large portion of photons undergo Compton scattering interactions and produce scattered radiation. Most scattered radiation is produced omnidirectionally and recorded by pixels on the area detector; it does not reflect the actual attenuation of an object along a specific path of the x-ray beam. The additional recorded x-ray attenuation reflecting nonlinear attenuation is called noise and contributes to image degradation. The total of scattered radiation is generally proportional to the total mass of tissue contained within the primary x-ray beam. Scattered radiation increases with increasing object thickness and field size. The contribution of this radiation to produce CBCT image may be greater than the primary beam. The scatter to primary radiation ratios for single-ray CT are about 0.01, 0.05 to 0.15 for fan beam and spiral CT and may be 0.4 to 2 in CBCT.

Other sources of image noise in CBCT are variations in the homogeneity of the incident x-ray beam (quantum mottle) and noise of the detector system (electronic). The inhomogeneity of x-ray photons depends on the number of the primary and scattered x-ray absorbed, x-ray spectra incident on the detector and the number of projections. Added noise from detector is due to the inherent degradations of the detector system related to the x-ray absorption efficiency of energy at the detector.

Furthermore, there is a pronounced heel effect because of the increased divergence of the x-ray beam over the area detector. This produces a large variation or nonuniformity of the incident x-ray beam on the patient and resultant nonuniformity in absorption with greater signal to noise ratio on the cathode side of the image relative to the anode side.

B) Poor soft tissue contrast

Contrast is the spatial variation of the x-ray photon intensities that are transmitted through the patient. Therefore contrast gives a measure of difference between regions in an image. The variation in transmitted intensities is a result of differential attenuation of x-rays by tissues which differ in density, atomic number and thickness. There are two principal factors that limit the contrast resolution of CBCT. The scattered radiation not only contributes noise of the image, it is also an important factor in reducing the contrast of the cone beam system. X-ray scatter reduces subject contrast by adding background signals, therefore it reduces image quality. Another factor is inherent flat panel detector based artifacts that affect its linearity or response to x-radiation.

2.2 Review of Related Literatures

2.2.1. The accuracy of linear measurements

Lascala et al.[14] evaluated the accuracy of linear measurements obtained by CBCT images using NewTom 9000 (Quantitative Radiology, Verona, Italy). Thirteen anatomical sites in eight dry skulls were measured using a caliper as real measurements. The results showed that the real measurements were always larger than those of the CBCT images but these differences were only significant for measurements of the internal structures of the skull base. The conclusion was that although measurements on the CBCT images underestimated the real distances of the skull base, it was reliable for linear measurements of other structures in dentomaxillofacial region with the CBCT images.

Kamburoglu et al.[15] assessed the accuracy and reproducibility of CBCT measurements of a human dry skull by comparing them to direct digital caliper measurements by three trained observers. Heated gutta percha was used to mark specific distances on a human skull. CBCT images were obtained with Iluma (3M Imtec, Oklahoma, USA) and 3D Accuitomo 170 (J.Morita Mfg.Corp., Kyoto, Japan). In addition, 3D reconstructions were produced from images obtained from both machines. All measurements were made independently by three trained observers and were repeated after an interval of 1 week. Agreement between observers and image type was assessed by calculating Pearson correlation coefficients, with a level of significance at $p<0.05$. This study revealed that the intraclass correlations coefficients between the intra- and inter-observer reading showed almost perfect. Pearson correlation coefficients (r) ranged from 0.995 to 1 for the first and second measurements of each observer. Correlations among observer were also very high, ranging from 0.992 to 1 for both the first and second reading for different image types. The results showed that the CBCT image measurements were identical and highly correlated with the gold standard direct digital caliper measurements. In addition, accuracy of measurements in various distances on a human skull obtained from different CBCT units and image types is comparable to that of digital caliper measurements. They concluded that all 2D and 3D images obtained with the Iluma and 3D Accuitomo 170 CBCT units performed similarly in terms of accuracy and reproducibility of measurements of predetermined mandibular, maxillary, and skull-base distances, without differences in intra-observer or inter-observer agreement. Therefore, they recommended the use of CBCT in the measurement of the dentomaxillofacial region.

2.2.2. The dimensional stability

Kopp and Ottl [16] evaluated the dimensional stability in composite CBCT. The Kodak 9000 3D system with stitching software which can combine up to three component volumes to yield a larger composite volume was used for the evaluation of a human mandible with three endodontic instruments as markers. The distances between several points were measured directly and compared with the values measured on screen. Displacements of the mandible along all axes between exposures as well as angular displacements were conducted to test the capability of the system. They found that the dimensional stability was acceptable even when the mandible was scanned with different angulations.

El-Beialy et al.[17] determined the accuracy and reliability of measurements obtained from 3D CBCT for different head orientations. Stainless steel wires were fixed to a dry skull at different places. The skull was scanned by using the Galileos (Sirona, Bensheim, Germany) CBCT in the centered and 5 other positions. Intra-observer and inter-observer reliability tests were performed by using 6 landmarks identified on the virtual 3D skulls by two operators. Two methods were used to determine the accuracy of measurements on the virtual 3D skull scanned in different positions. In the first method, 12 linear distances were compared on the physical skull and the 3D virtual skull in the centered and the other scanning positions. In the second method, registration of each of the 5 positions on the centered position was done separately and coordinates of 11 landmarks were identified in each position and compared with the centered position. Data gathered from two methods were compared statistically. This study revealed that concordance correlation and Pearson correlation coefficients values were almost 0.9999 in all comparisons denoting: (1) high intra-observer and inter-observer reliability; (2) very high concordance between the physical skull and the CBCT centered position measurements; (3) very high concordance between measurements of the centered position in relation to those obtained from the different skull positions; and (4) registration of the skulls in the different positions showed high concordance, with the highest values between the centered and off-centered positions and the lowest with the complex position. They concluded that accuracy and reliability of CBCT measurements are not affected by changing the skull orientation.

2.2.3. Other studies in Kodak 9000 3D

Three studies with Kodak 9000 3D system have been documented.

Zhang et al.[18] evaluated the accuracy of CBCT for the detection of noncavitated proximal caries and compared the detection accuracies of 2 CBCT imaging systems with those based on plain-film radiographs and phosphor-plate images. Test radiographs of 39 noncavitated unrestored human permanent teeth were obtained with film, phosphor-plate, ProMax 3D (Planmeca Oy, Helsinki, Finland) and Kodak 9000 3D imaging systems. Seven observers used a 5-level scale to evaluate test images for the presence of proximal caries. With histologic examination serving as the reference standard, observer performances were assessed with receiver operating characteristic (ROC) curves, and the areas under the ROC curves (A(z) values) for the observers and modalities were analyzed with a repeated-measures analysis of variance. The results showed that the mean A(z) values for film, phosphor plates, ProMax 3D and Kodak 9000 3D imaging systems were 0.541, 0.523, 0.528 and 0.525 respectively. They concluded that for detecting subtle noncavitated proximal caries, the detection accuracy with the CBCT images was little better than chance performance and was similar to that with phosphor plate- and film-based intraoral images.

Qu et al.[19] reported the caries detection accuracy on CBCT images. They evaluated the diagnostic accuracy of approximal carious lesions among five CBCT systems and assessed the effect of detector types employed by different CBCT systems on the accuracy of approximal caries diagnosis. Thirty-nine extracted noncavitated human permanent teeth were employed in the study. The clinical appearance of the tooth surface after cleaning ranged from sound to discolored with white/brown discolorations. Seven observers evaluated 78 approximal surfaces of the teeth with respect to caries by the images from five CBCT systems: (1) NewTom 9000 (Quantitative Radiology, Verona, Italy); (2) Accuitomo 3DX (J.Morita Mfg.Corp., Kyoto, Japan); (3) Kodak 9000 3D; (4) ProMax 3D (Planmeca Oy, Helsinki, Finland); and (5) DCT PRO (Vatech Co., Ltd., Yongin-Si, South Korea). The NewTom 9000 and the Accuitomo 3DX used detector of II and CCD type while the other three systems used flat panel detector composed of Amorphous Silicon or Complementary Metal Oxide Semiconductor (CMOS). The lesions were validated by histological examination. The area under ROC curve (A(z)) was used to evaluate the diagnostic accuracy. This study revealed that microscopy of approximal surfaces found 47.4% sound, 39.8% enamel, and 12.8% dentin lesions. They concluded that the differences of A(z) values among five CBCT systems were not statistically significant. In addition, no significant difference was found between the two detector types of CBCT systems.

Another research was about validation of CBCT as a tool to explore root canal anatomy by **Michetti et al.**[20]. They compared the reconstructions of root canal systems given by the Kodak 9000 3D with histologic sections to evaluate the reliability of the reconstructions. Nine intact freshly extracted teeth with closed apexes were scanned by the Kodak 9000 3D. After reconstruction of the volumes, the outline of the root canals was defined by segmentation. Histologic sections were then made of each specimen at predetermined levels. After digitization, 2D cone beam reconstructions were compared with the outline of the canals obtained by histologic sections using areas and Feret's diameters. The statistical analysis was performed using the Pearson correlation coefficient. The result showed that strong to very strong correlation was found between the data acquired by using CBCT and histology: r (area) = 0.928; r (diameter) = 0.890. They found that the Kodak 9000 3D appears to be a very interesting, reliable and noninvasive measuring tool that can be used in all spatial planes.

CHAPTER III

RESEARCH METHODOLOGY

3.1 Research Design

This study is a cross-sectional analytical observational study.

3.2 Research Design Model (Figure 3.1)

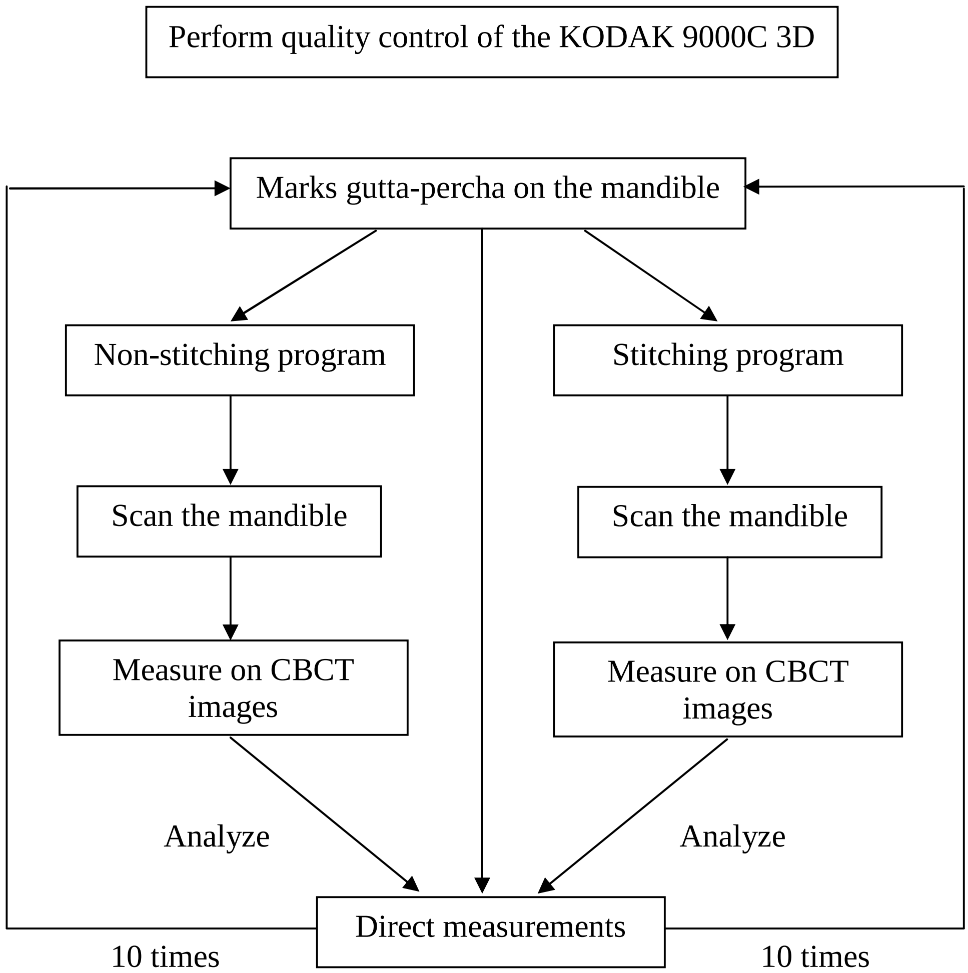

Figure 3.1 Research design model

3.3 Conceptual Framework (Figure 3.2)

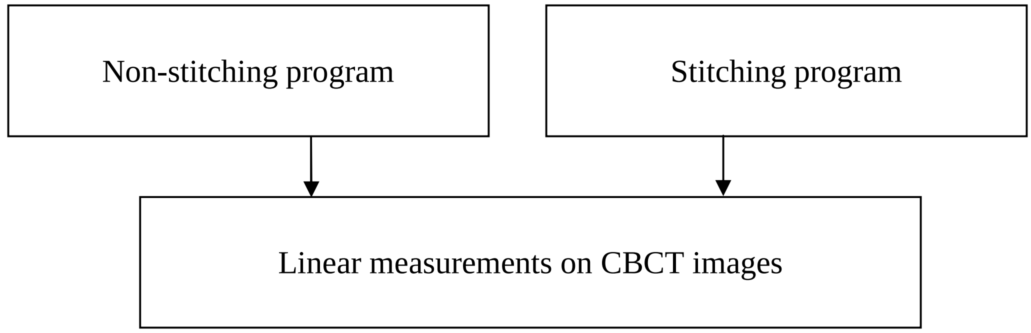

Figure 3.2 Conceptual Framework

3.4 Keywords

- CBCT
- Kodak 9000 3D
- Accuracy
- Stitching program

3.5 Research Question

Are there any differences of linear measurements from stitched and non-stitched CBCT images in comparison to direct measurements?

3.6 Materials

3.6.1 CBCT system (Figure 3.3)**:**

Model Kodak 9000C 3D

Figure 3.3 Kodak 9000C 3D CBCT system
(Carestream Health, Inc., New York, USA.)

3.6.2 Human dry mandibles 10 mandibles (Figure 3.4)**:**

The human dry mandibles were borrowed from Department of Anatomy, Faculty of Medicine Siriraj Hospital, Mahidol University

Figure 3.4 Human dry mandibles

Exclusion criteria of human dry mandibles

1. The teeth had metal or filling materials.
2. The teeth were primary dentition.

3.6.3 Gutta-percha size 80 (Figure 3.5)**:**

Figure 3.5 Gutta-percha

3.6.4 Digital caliper (Figure 3.6)**:**

Mitutoyo's absolute Digimatic Caliper Series 500

Figure 3.6 Mitutoyo's absolute Digimatic Caliper Series 500 (Mitutoyo Corp., Kanagawa, Japan)

3.7 Methods

3.7.1 Perform quality control of CBCT system.

3.7.2 Cut gutta-percha into 1 mm length and place at

1) The lingual bone at the level of superior border of the mental foramen on the left and right sides.

2) The distobuccal alveolar crest of the left and right first molar teeth.

3) The distolingual alveolar crest of the left and right first molar teeth.

4) The most inferior point of the mandible on the left and right sides perpendicular to the gutta-percha indicated in no.2.

5) The labial bone at the level of superior border of the lingual foramen.

3.7.3 Place gutta-percha rod to the following positions

1) From the buccal alveolar bone to superior border of the left and right mental foramen.

2) From the lingual alveolar crest at the midline to superior border of the lingual foramen.

These markers make five vertical distances (Figure 3.7) from

1) The buccal alveolar bone to superior border of the right mental foramen.

2) The distobuccal alveolar bone of the right first molar tooth perpendicular to the most inferior point of the mandible on the right side.

3) The buccal alveolar bone to superior border of the left mental foramen.

4) The distobuccal alveolar bone of the left first molar tooth perpendicular to the most inferior point of the mandible on the left side.

5) The lingual alveolar crest to superior border of the lingual foramen.

These markers make five horizontal distances (Figure 3.7) from

1) Bone width at the level of superior border of the mental foramen on the right side.

2) The distobuccal alveolar bone of the right first molar teeth to the distolingual alveolar bone of the right first molar tooth.

3) Bone width at the level of superior border of the mental foramen on the left side.

4) The distobuccal alveolar bone of the left first molar teeth to the distolingual alveolar bone of the left first molar tooth.

5) Bone width at the level of the superior border of the lingual foramen.

3.7.4 Measure all distances of the mandible directly using digital caliper three times on three different days, then average the measured values.

3.7.5 Position the mandible in the CBCT machine using styrofoam holder (Figure 3.8)

3.7.6 Scan the mandible using stitching and non-stitching programs at 70 kVp, 3.2 mA

3.7.7 Measure all distances on CBCT images obtained by using and not using stitching program three times on three different days, then average the values.

3.7.8 Compare the measurements from CBCT images with direct measurements

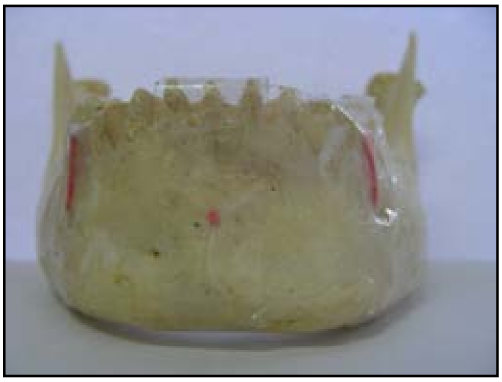
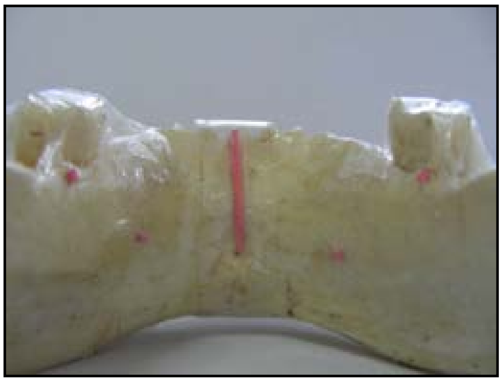

(a) (b)


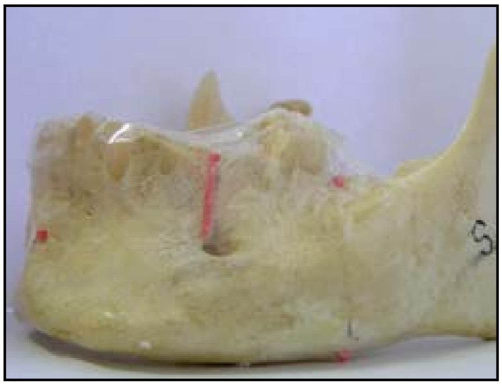

(c) (d)

(e)

Figure 3.7 Mark the vertical and horizontal distances with gutta-percha
(a) Labial aspect (b) Lingual aspect (c) Right aspect
(d) Left aspect (e) Occlusal aspect

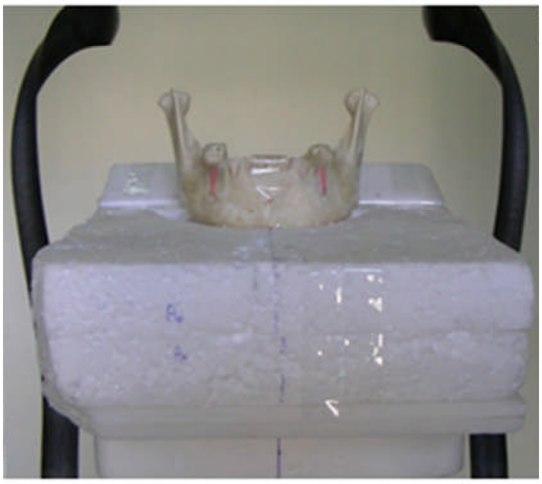

Figure 3.8 Place the mandible in the CBCT machine

3.8 Data Analysis

Vertical and horizontal distances from direct measurements, stitched CBCT images, and non-stitched CBCT images were reported as mean, standard deviation (SD) and error in comparison to direct measurements presented in tables

The accuracy of linear measurements between using stitching and non-stitching programs were compared to the direct measurements reported as Intraclass Correlation Coefficients (ICCs) in tables.

3.9 Sample Size Determination

Sample size is number of the mandibles determined by program PASS for testing ICCs at Power 0.9, Alpha 0.05, and Intraclass Correlation 0.8. Number of mandibles are nine. Calculation Error is 10%. Therefore, ten mandibles are required.

3.10 Statistical Analysis

3.10.1 Descriptive statistic: mean, SD and error were performed using Microsoft excels.

3.10.2 The ICCs between direct measurements and non-stitched CBCT images and between direct measurements and stitched CBCT images were calculated using Statistical Package for Social Science (SPSS) program version 16.0.

3.11 Outcome Measurement

The vertical and horizontal distances from CBCT images using stitching and non-stitching programs and direct measurements.

3.12 Expected Benefits

The accuracy of linear measurements using stitching and non-stitching programs on CBCT Kodak 9000C 3D in comparison to direct measurements is determined. These would be benefit to the oral radiologists for consideration of using stitching program.

3.13 Ethical Considerations

Although only human dry mandibles were studied, the ethical consideration had already been proposed and approved by the Ethics Committee of Faculty of Medicine, Chulalongkorn University and Siriraj Institutional Review Board (SIRB), Mahidol University.

CHAPTER IV

RESULTS

4.1 Quality control of the CBCT system: KODAK 9000C 3D

The results of quality control were shown in Appendix B.

4.2 Measurement of vertical and horizontal distances

The means and standard deviations of vertical and horizontal distances from direct measurements, non-stitched CBCT images and stitched CBCT images in each mandible were shown in Table 4.1-4.10.

Table 4.1 Means and standard deviations of vertical and horizontal distances from direct measurements, non-stitched CBCT images and stitched CBCT images in mandible number (no) 1

		Direct measurements (mm)	Non-stitched CBCT images (mm)	Stitched CBCT images (mm)
Vertical	1	12.03±0.16	12.33±0.12	12.43±0.06
	2	22.89±0.13	22.60±0.10	22.37±0.15
	3	11.68±0.27	11.63±0.06	11.67±0.35
	4	23.77±0.26	23.80±0.00	23.77±0.06
	5	19.15±0.13	18.93±0.21	18.97±0.06
Horizontal	1	12.47±0.04	11.97±0.06	12.07±0.15
	2	11.20±0.31	11.67±0.15	11.43±0.12
	3	12.07±0.05	11.83±0.06	11.93±0.12
	4	10.54±0.12	11.20±0.00	11.30±0.10
	5	11.43±0.05	11.37±0.12	11.17±0.23

Table 4.2 Means and standard deviations of vertical and horizontal distances from direct measurements, non-stitched CBCT images and stitched CBCT images in mandible no.2

		Direct measurements (mm)	Non-stitched CBCT images (mm)	Stitched CBCT images (mm)
Vertical	1	5.97±0.04	5.90±0.00	5.93±0.06
	2	19.96±0.13	19.80±0.10	19.83±0.06
	3	11.22±0.10	11.27±0.06	11.23±0.06
	4	17.02±0.10	16.90±0.20	16.77±0.06
	5	18.39±0.10	18.30±0.10	18.33±0.06
Horizontal	1	9.97±0.06	9.97±0.06	10.03±0.06
	2	7.65±0.09	7.60±0.10	7.63±0.06
	3	10.04±0.08	10.00±0.17	10.17±0.12
	4	9.40±0.07	9.30±0.10	9.27±0.15
	5	10.48±0.05	10.40±0.10	10.57±0.06

Table 4.3 Means and standard deviations of vertical and horizontal distances from direct measurements, non-stitched CBCT images and stitched CBCT images in mandible no.3

		Direct measurements (mm)	Non-stitched CBCT images (mm)	Stitched CBCT images (mm)
Vertical	1	11.54±0.08	11.43±0.06	11.47±0.06
	2	24.14±0.19	23.83±0.12	23.80±0.00
	3	11.14±0.02	11.07±0.06	11.13±0.06
	4	21.46±0.02	20.90±0.10	20.90±0.10
	5	12.93±0.02	12.63±0.06	12.73±0.06
Horizontal	1	10.83±0.07	10.57±0.06	10.60±0.10
	2	9.53±0.05	9.47±0.06	9.53±0.12
	3	11.15±0.06	11.03±0.06	11.13±0.06
	4	11.17±0.05	10.53±0.06	10.60±0.10
	5	11.25±0.11	11.47±0.12	11.40±0.00

Table 4.4 Means and standard deviations of vertical and horizontal distances from direct measurements, non-stitched CBCT images and stitched CBCT images in mandible no.4

		Direct measurements (mm)	Non-stitched CBCT images (mm)	Stitched CBCT images (mm)
Vertical	1	11.47±0.11	11.33±0.12	11.47±0.15
	2	21.97±0.32	21.00±0.10	21.17±0.06
	3	9.68±0.11	9.93±0.12	10.20±0.17
	4	19.28±0.49	18.90±0.10	19.00±0.10
	5	18.57±0.20	18.47±0.12	18.00±0.10
Horizontal	1	11.28±0.45	10.77±0.06	11.13±0.12
	2	10.27±0.24	10.57±0.15	10.77±0.06
	3	11.42±0.37	10.23±0.06	10.40±0.10
	4	11.79±0.40	11.37±0.15	11.47±0.12
	5	10.99±0.13	10.80±0.10	10.87±0.06

Table 4.5 Means and standard deviations of vertical and horizontal distances from direct measurements, non-stitched CBCT images and stitched CBCT images in mandible no.5

		Direct measurements (mm)	Non-stitched CBCT images (mm)	Stitched CBCT images (mm)
Vertical	1	13.00±0.16	12.97±0.06	13.33±0.15
	2	24.79±0.59	24.57±0.12	24.63±0.06
	3	11.79±0.25	12.33±0.06	12.70±0.10
	4	25.24±0.37	25.10±0.10	25.23±0.06
	5	20.97±0.36	20.63±0.12	20.47±0.12
Horizontal	1	10.65±0.31	10.03±0.12	9.83±0.15
	2	10.75±1.03	11.93±0.06	11.97±0.06
	3	10.55±0.37	10.10±0.10	9.97±0.12
	4	9.97±0.28	10.00±0.10	10.27±0.12
	5	15.53±0.14	16.20±0.17	16.37±0.15

Table 4.6 Means and standard deviations of vertical and horizontal distances from direct measurements, non-stitched CBCT images, and stitched CBCT images in mandible no.6

		Direct measurements (mm)	Non-stitched CBCT images (mm)	Stitched CBCT images (mm)
Vertical	1	14.35±0.24	14.00±0.20	14.10±0.00
	2	30.17±0.12	29.23±0.06	29.43±0.15
	3	13.47±0.04	13.33±0.06	13.43±0.06
	4	29.65±0.31	29.30±0.10	29.17±0.06
	5	21.81±0.11	21.63±0.06	21.83±0.23
Horizontal	1	13.54±0.15	13.13±0.06	13.23±0.21
	2	10.13±0.47	9.97±0.06	9.83±0.15
	3	12.43±0.12	12.10±0.10	12.03±0.21
	4	10.00±0.14	10.23±0.15	10.33±0.06
	5	12.85±0.27	13.90±0.17	13.93±0.15

Table 4.7 Means and standard deviations of vertical and horizontal distances from direct measurements, non-stitched CBCT images, and stitched CBCT images in mandible no.7

		Direct measurements (mm)	Non-stitched CBCT images (mm)	Stitched CBCT images (mm)
Vertical	1	14.47±0.14	14.23±0.15	14.13±0.06
	2	27.15±0.08	27.17±0.06	27.27±0.15
	3	14.02±0.03	14.03±0.06	13.83±0.31
	4	24.65±0.08	23.67±0.06	23.60±0.10
	5	27.31±0.08	27.23±0.06	27.57±0.06
Horizontal	1	16.64±0.02	16.33±0.06	16.43±0.12
	2	13.90±0.47	13.97±0.06	13.77±0.06
	3	15.86±0.03	15.63±0.06	15.83±0.06
	4	16.26±0.06	16.00±0.10	15.93±0.06
	5	17.42±0.07	17.10±0.00	17.10±0.17

Table 4.8 Means and standard deviations of vertical and horizontal distances from direct measurements, non-stitched CBCT images, and stitched CBCT images in mandible no.8

		Direct measurements (mm)	Non-stitched CBCT images (mm)	Stitched CBCT images (mm)
Vertical	1	12.74±0.09	12.67±0.06	12.53±0.15
	2	18.40±0.36	17.63±0.06	17.67±0.06
	3	10.33±0.02	10.33±0.12	10.43±0.12
	4	20.77±0.26	20.37±0.06	20.50±0.00
	5	15.75±0.03	15.53±0.12	15.57±0.06
Horizontal	1	12.02±0.12	12.00±0.00	11.97±0.06
	2	11.90±0.38	12.03±0.12	12.20±0.10
	3	11.18±0.24	10.73±0.06	10.60±0.00
	4	9.19±0.25	9.10±0.17	9.03±0.21
	5	11.23±0.02	11.67±0.06	11.70±0.10

Table 4.9 Means and standard deviations of vertical and horizontal distances from direct measurements, non-stitched CBCT images, and stitched CBCT images in mandible no.9

		Direct measurements (mm)	Non-stitched CBCT images (mm)	Stitched CBCT images (mm)
Vertical	1	15.11±0.07	15.03±0.06	15.07±0.12
	2	26.27±0.12	26.13±0.06	25.93±0.12
	3	14.87±0.05	14.97±0.06	14.97±0.12
	4	28.37±0.08	28.07±0.12	28.03±0.21
	5	23.73±0.03	23.37±0.06	23.33±0.06
Horizontal	1	14.63±0.03	14.17±0.06	14.03±0.06
	2	12.37±0.10	12.37±0.06	12.37±0.06
	3	14.65±0.08	14.10±0.17	14.30±0.17
	4	13.15±0.13	12.97±0.12	13.17±0.06
	5	13.94±0.10	13.90±0.10	13.93±0.15

Table 4.10 Means and standard deviations of vertical and horizontal distances from direct measurements, non-stitched CBCT images, and stitched CBCT images in mandible no.10

		Direct measurements (mm)	Non-stitched CBCT images (mm)	Stitched CBCT images (mm)
Vertical	1	14.14±0.05	14.17±0.06	14.10±0.10
	2	24.22±0.12	24.17±0.06	24.13±0.06
	3	13.21±0.05	13.17±0.12	13.17±0.06
	4	23.90±0.23	24.00±0.10	23.83±0.12
	5	18.90±0.01	18.63±0.06	18.60±0.10
Horizontal	1	13.54±0.02	12.43±0.06	12.67±0.06
	2	11.07±0.19	10.90±0.00	10.93±0.12
	3	13.09±0.01	12.23±0.12	12.27±0.06
	4	11.10±0.28	10.87±0.12	10.93±0.12
	5	11.76±0.05	11.83±0.12	11.70±0.00

The errors of non-stitched CBCT images and stitched CBCT images compared to direct measurements in each mandible were shown in Table 4.11 and 4.12, respectively.

Table 4.11 The errors between direct measurements and non-stitched CBCT images in each mandible

		Errors (mm)				
		Mandible no.				
		1	2	3	4	5
Vertical	1	-0.30	0.07	0.11	0.14	0.03
	2	0.29	0.16	0.31	0.97	0.22
	3	0.05	-0.04	0.07	-0.25	-0.54
	4	-0.03	0.12	0.56	0.38	0.14
	5	0.22	0.09	0.30	0.10	0.34
Horizontal	1	0.50	0.00	0.26	0.51	0.62
	2	-0.47	0.05	0.06	-0.30	-1.18
	3	0.24	0.04	0.12	1.19	0.45
	4	-0.66	0.10	0.64	0.42	-0.03
	5	0.06	0.08	-0.22	0.19	-0.67
		Mandible no.				
		6	7	8	9	10
Vertical	1	0.35	0.24	0.07	0.08	-0.03
	2	0.94	-0.02	0.77	0.14	0.05
	3	0.14	-0.01	0.00	-0.10	0.04
	4	0.35	0.98	0.40	0.30	-0.10
	5	0.18	0.08	0.22	0.36	0.27
Horizontal	1	0.41	0.31	0.02	0.46	1.11
	2	0.16	-0.07	-0.13	0.00	0.17
	3	0.33	0.23	0.45	0.55	0.86
	4	-0.23	0.26	0.09	0.18	0.23
	5	-1.05	0.32	-0.44	0.04	-0.07

Table 4.12 The errors between direct measurements and stitched CBCT images in each mandible

		Errors (mm)				
		Mandible no.				
		1	2	3	4	5
Vertical	1	-0.40	0.04	0.07	0.00	-0.33
	2	0.52	0.13	0.34	0.80	0.16
	3	0.01	-0.01	0.01	-0.52	-0.91
	4	0.00	0.25	0.56	0.28	0.01
	5	0.18	0.06	0.20	0.57	0.50
Horizontal	1	0.40	-0.06	0.23	0.15	0.82
	2	-0.23	0.02	0.00	-0.50	-1.22
	3	0.14	-0.13	0.02	1.02	0.58
	4	-0.76	0.13	0.57	0.32	-0.30
	5	0.26	-0.09	-0.15	0.12	-0.84
		Mandible no.				
		6	7	8	9	10
Vertical	1	0.35	0.34	0.21	0.04	0.04
	2	0.74	-0.12	0.73	0.34	0.09
	3	0.04	0.19	0.00	-0.10	0.04
	4	0.48	1.05	0.27	0.34	0.07
	5	-0.02	-0.26	0.18	0.40	0.30
Horizontal	1	0.31	0.21	0.05	0.60	0.87
	2	0.30	0.13	-0.30	0.00	0.14
	3	0.40	0.03	0.00	0.35	0.82
	4	-0.33	0.33	0.16	-0.02	0.17
	5	-1.08	0.32	-0.47	0.01	0.06

4.3 Test of accuracy of linear measurements between using stitching and non-stitching programs

The ICCs of intra-observer reliability and inter-method reliability were computed and presented in Table 4.13 and 4.14, respectively

Table 4.13 The ICCs of intra-observer reliability

Mandible no.	ICCs of each measurement		
	Direct	Non-stitched CBCT images	Stitched CBCT images
1	1.000	1.000	1.000
2	1.000	1.000	1.000
3	1.000	1.000	1.000
4	0.998	1.000	1.000
5	0.999	1.000	1.000
6	1.000	1.000	1.000
7	1.000	1.000	1.000
8	0.999	1.000	1.000
9	1.000	1.000	1.000
10	1.000	1.000	1.000

Table 4.14 The ICCs of inter-method reliability

Distances		ICCs between Direct measurements and Non-Stitched CBCT images	ICCs between Direct measurements and Stitched CBCT images
Vertical	1	0.998	0.998
	2	0.994	0.996
	3	0.993	0.980
	4	0.997	0.997
	5	1.000	0.998
Horizontal	1	0.988	0.988
	2	0.972	0.967
	3	0.982	0.980
	4	0.985	0.982
	5	0.983	0.980

Table 4.13 showed that the ICCs were 0.998 to 1.000 in direct measurements. All ICCs of both non-stitched CBCT images and stitched CBCT images were 1.000 indicated strong agreement between duplicated measurements made by a single observer.

Table 4.14 revealed that the ICCs of inter-method reliability were 0.972 to 1.000 in direct measurements versus non-stitched CBCT images and 0.967 to 0.998 in direct measurements versus stitched CBCT images. These results showed that measurements from non-stitched CBCT images were slightly more accurate than stitched CBCT images. However, there were no statistically significant differences between direct measurements and stitched CBCT images or non-stitched CBCT images ($P > 0.05$).

CHAPTER V

DISCUSSION AND CONCLUSIONS

5.1 Discussion

CBCT has become an important imaging method for evaluation of oral and maxillofacial structures. The accuracy of linear measurements on CBCT images is necessary for treatment in this region especially for implant placement. Nowadays CBCT system with various imaging software are available. Previous studies the geometric accuracy of CBCT system have been reported.[14, 15, 21, 22] These studies showed the measurements from CBCT images were statistically similar to direct measurements. The present study evaluates the linear measurements on stitched and non-stitched CBCT images using Kodak 9000C 3D systems compared to direct measurements. The results show that linear measurements on both CBCT images were highly accurate without statistical difference when compared to direct measurements ($P>0.05$). However, non-stitched CBCT images are slightly more accurate than stitched CBCT images. The accuracy of linear measurements from stitched CBCT images in this study is in agreement with a previous report by Kopp and Ottl.[16] In their study, they evaluated the dimensional stability in Kodak 9000 3D CBCT system with stitching software, and concluded that the stitching software was a useful tool to yield larger FOV. The dimensional stability was acceptable when rotated the mandible. Therefore, displacement of the mandible in x axis or y axis did not affect linear measurements.

Most of the errors between direct measurements and non-stitched CBCT images and between direct measurements and stitched CBCT images are positive values. These indicate that the distances measured from direct measurements are longer than those measured on CBCT images. The underestimation on CBCT images might be because the measurements on CBCT images are made in truly cross-sectional areas, whereas direct measurements are performed in the mandibles with some convex surfaces. These results are in accordance with a previous study by

Lascala et al.[14] which showed that the real distances measured on dry skulls were always larger than those obtained from the CBCT images.

Most of the errors between direct measurements and non-stitched CBCT images and between direct measurements and stitched CBCT images are less than $\pm$1 mm. The errors between direct measurements and non-stitched CBCT images which are larger than 1 mm are found in the third horizontal distances of the mandible no.4 and the first horizontal distances of the mandible no.10. The errors between direct measurements and stitched CBCT images which are larger than 1 mm are also found in the third horizontal distances of the mandible no.4. The errors between direct measurements and non-stitched CBCT images and between direct measurements and stitched CBCT images which are less than 1 mm are found in the second horizontal distances of the mandible no.5 and the fifth horizontal distances of the mandible no.6. It can be concluded that results suggest that the anatomy of the mandible might have an effect on linear measurements.

It has been stated that the measurement errors for dental implant planning from the radiographs should not exceed 1 mm.[23] In this study, most measurement errors are acceptable of less than 1 mm.

The ICCs in non-stitched, stitched CBCT images and direct measurements of vertical distances are slightly higher than those of horizontal distances. This indicates that the measurements in vertical orientation are more accurate than those in horizontal orientation. However, the differences are not statistically significant.

Because the stitched CBCT images yield accurate measurements with larger image area, this technique should be applied in clinical evaluation of the patient. However, the stitching program requires longer imaging time which can lead to blurring artifact from patient’s movement during imaging procedure.

The limitation of this study is all measurements were made by single observer. Bias might be occurred although the measurements were made three times and the observer did not exactly know the direct measurements from digital caliper.

5.2 Conclusions

Stitching program in KODAK 9000C 3D CBCT system provides images with larger area making image analysis of the multiple areas in a single evaluation possible. This study showed that stitching program is accurate for evaluation of linear measurements. Therefore, this program could lead to more convenient and effective treatment planning in many clinical applications.

REFERENCES

[1] Stuart, C.W., and Michael, J.P. Oral Radiology Principles and Interpretation. 6th ed. St. Louis: Mosby, 2009.

[2] Baily, N.A., Keller, R.A., Jakowatz, C.V., and Kak, A.C. The capability of fluoroscopic systems for the production of computerized axial tomograms. Invest Radiol 11 (1976): 434-9.

[3] Harrison, R.M., and Farmer, F.T. The determination of anatomical cross-sections using a radiotherapy simulator. Br J Radiol 51 (1978): 448-53.

[4] Cho, P.S., Johnson, R.H., and Griffin, T.W. Cone-beam CT for radiotherapy applications. Phys Med Biol 40 (1995): 1863-83.

[5] Robb, R.A. The Dynamic Spatial Reconstructor: An X-Ray Video-Fluoroscopic CT Scanner for Dynamic Volume Imaging of Moving Organs. IEEE Trans Med Imaging 1 (1982): 22-33.

[6] Machin, K., and Webb, S. Cone-beam x-ray microtomography of small specimens. Phys Med Biol 39 (1994): 1639-57.

[7] Mozzo, P., Procacci, C., Tacconi, A., Martini, P.T., and Andreis, I.A. A new volumetric CT machine for dental imaging based on the cone-beam technique: preliminary results. Eur Radiol 8 (1998): 1558-64.

[8] Arai, Y., Tammisalo, E., Iwai, K., Hashimoto, K., and Shinoda, K. Development of a compact computed tomographic apparatus for dental use. Dentomaxillofac Radiol 28 (1999): 245-8.

[9] Schulze, D., Heiland, M., Thurmann, H., and Adam, G. Radiation exposure during midfacial imaging using 4- and 16-slice computed tomography, cone beam computed tomography systems and conventional radiography. Dentomaxillofac Radiol 33 (2004): 83-6.

[10] Tsiklakis, K., Donta, C., Gavala, S., Karayianni, K., Kamenopoulou, V., and Hourdakis, C.J. Dose reduction in maxillofacial imaging using low dose Cone Beam CT. Eur J Radiol 56 (2005): 413-7.

[11] Sukovic, P. Cone beam computed tomography in craniofacial imaging. Orthod Craniofac Res 6(Suppl 1) (2003): 31-6.

[12] Gupta, R. et al. Ultra-high resolution flat-panel volume CT: fundamental principles, design architecture, and system characterization. Eur Radiol 16 (2006): 1191-205.

[13] Baba, R., Konno, Y., Ueda, K., and Ikeda, S. Comparison of flat-panel detector and image-intensifier detector for cone-beam CT. Comput Med Imaging Graph 26 (2002): 153-8.

[14] Lascala, C.A., Panella, J., and Marques, M.M. Analysis of the accuracy of linear measurements obtained by cone beam computed tomography (CBCT-NewTom). Dentomaxillofac Radiol 33 (2004): 291-4.

[15] Kamburoglu, K., Kolsuz, E., Kurt, H., Kilic, C., Ozen, T., and Paksoy, C.S. Accuracy of CBCT measurements of a human skull. J Digit Imaging 24 (2011): 787-93.

[16] Kopp, S., and Ottl, P. Dimensional stability in composite cone beam computed tomography. Dentomaxillofac Radiol 39 (2010): 512-6.

[17] El-Beialy, A.R., Fayed, M.S., El-Bialy, A.M., and Mostafa, Y.A. Accuracy and reliability of cone-beam computed tomography measurements: Influence of head orientation. Am J Orthod Dentofacial Orthop 140 (2011): 157-65.

[18] Zhang, Z.L., Qu, X.M., Li, G., Zhang, Z.Y., and Ma, X.C. The detection accuracies for proximal caries by cone-beam computerized tomography, film, and phosphor plates. Oral Surg Oral Med Oral Pathol Oral Radiol Endod 111 (2011): 103-8.

[19] Qu, X., Li, G., Zhang, Z., and Ma, X. Detection accuracy of in vitro approximal caries by cone beam computed tomography images. Eur J Radiol 79 (2011): e24-7.

[20] Michetti, J., Maret, D., Mallet, J.P., and Diemer, F. Validation of cone beam computed tomography as a tool to explore root canal anatomy. J Endod 36 (2010): 1187-90.

[21] Ganguly, R., Ruprecht, A., Vincent, S., Hellstein, J., Timmons, S., and Qian, F. Accuracy of linear measurement in the Galileos cone beam computed tomography under simulated clinical conditions. Dentomaxillofac Radiol 40 (2011): 299-305.

[22] Stratemann, S., Huang, J., Maki, K., Miller, A., and Hatcher, D. Comparison of cone beam computed tomography imaging with physical measures. Dentomaxillofac Radiol 37 (2008): 80-93.

[23] Wyatt, C.C., and Pharoah, M.J. Imaging techniques and image interpretation for dental implant treatment. Int J Prosthodont 11 (1998): 442-52.

APPENDICES

Appendix A: Case Record Form

Data Collection form of measurements

Mandible No.: ________ Measurements: Direct, Non-stitched, Stitched

Date: ________ Times (1st, 2nd, 3rd): ________________________

		Distance (mm)
Vertical	1	
	2	
	3	
	4	
	5	
Horizontal	1	
	2	
	3	
	4	
	5	

Appendix B: Quality control of the CBCT scanner

1. Beam quality or Half-value layer (HVL) measurement

Dosimeter: UNFORS MODEL Xi

Method: Set the distance from x-ray source to detector at 60 cm. The HVL was determined at 60, 70, and 80 kVp.

Results:

Set kVp	HVL (mm Al)	Average HVL (mm Al)	NCRP Report # 102 (mm Al)
60	2.18	2.19	-
	2.18		
	2.20		
70	2.59	2.59	At least 2.5
	2.59		
	2.60		
80	2.98	2.99	At least 2.5
	2.99		
	3.01		

Comments: Pass

2. Beam quantity, kVp linearity and kVp accuracy measurements

Method: Vary kVp from 60-80 in steps of 10 kVp. Set 5 mAs. Record the measured kVp and mGy. Compute mGy/mAs for each kVp setting.

Tolerance: The deviation should not exceed 5 kVp or 10% of set kVp.

Results:

Set kVp	Measured kVp	Average kVp	% Deviation	mGy	mGy/mAs
60	57.48	57.67	3.88	0.13	0.03
	57.72				
	57.83				
70	67.09	67.02	4.26	0.18	0.04
	67.04				
	66.92				
80	76.43	76.42	4.48	0.23	0.05
	76.34				
	76.48				

Comments: Pass

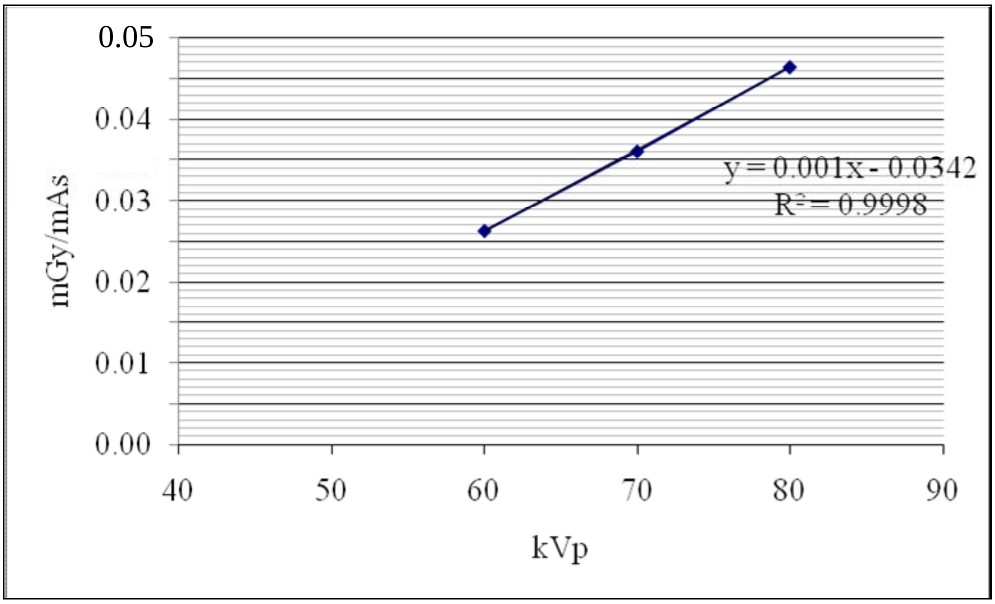

Figure I The linearity of the kVp and mGy/mAs

3. Exposure and kVp Consistency

Method: Set the distance from x-ray source to detector at 100 cm. Set 80 kVp

Tolerance: Coefficient of variation should be </= 0.05.

Results:

Set kVp	Measured kVp	Measured mGy
80	77.32	0.2325
	76.43	0.2327
	76.34	0.2313
	76.48	0.2325
Average	76.64	0.2323
SD	0.39	0.0006
CV	0.0051	0.0024

Comments: Pass

4. Image uniformity

Method: Image uniformity was measured with a CATPHAN phantom with a diameter of 20 cm, positioned at the patient's support. Using the eFilm™software, the mean pixel values were calculated in three slices at a central and four peripheral regions of interests (ROI) with an area of 50 mm^2.

Results:

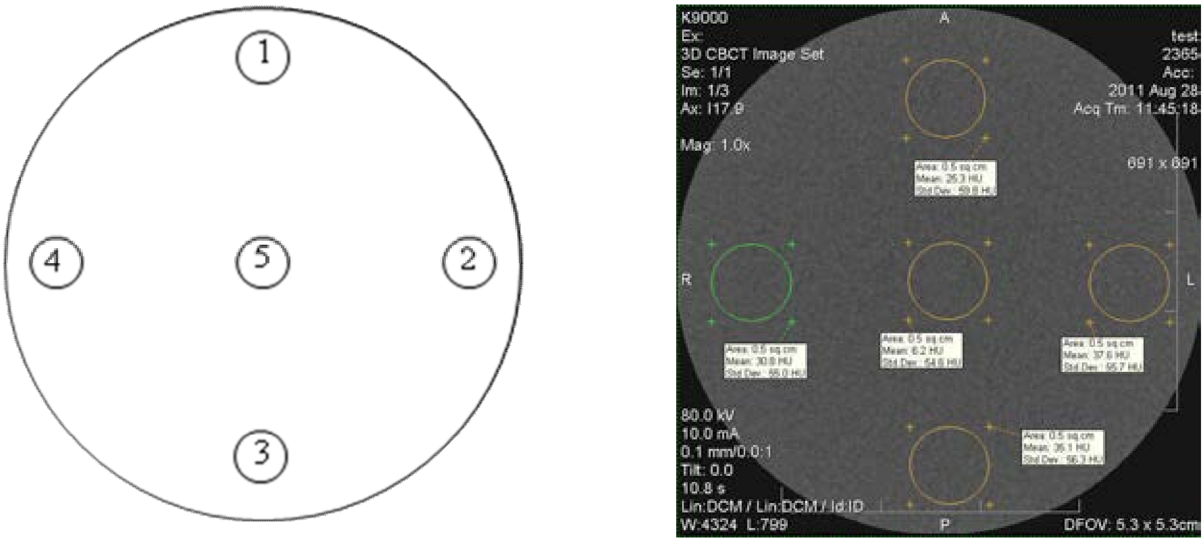

Figure II Position of ROI was measured the image uniformity

Position	Pixel values	Average
1	25.3	27.0
	28.6	
2	37.6	32.9
	28.2	
3	35.1	31.1
	27.1	
4	30.8	27.2
	23.6	
5	6.2	3.4
	0.5	

Comments: The mean pixel values of position 1-4 in all slices ranged from 27.0-32.9 with the mean of 29.6. At position 5 the mean pixel values were much less than the mean pixel values of other positions because of the x-ray attenuation.

5. Image artifact

Results: No finding image artifact on phantom image

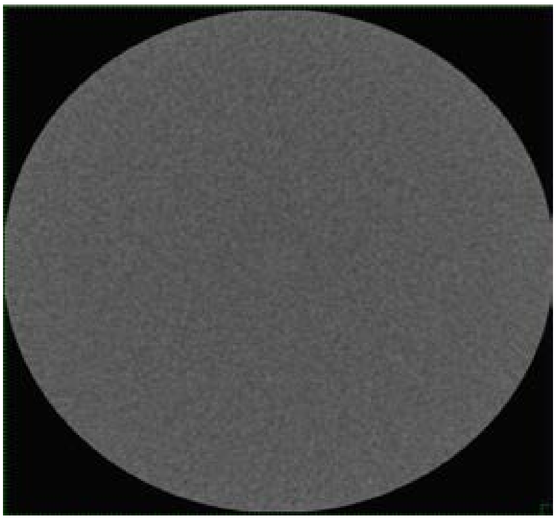

Figure III The phantom image

6. Radiation dose

Method: Radiation dose was measured using a CATPHAN phantom. The dose quantity in KODAK 9000C 3D CBCT system was obtained by the dose-area product (DAP) in unit of $mGycm^2$.

Results:

kVp	mA	Sec	mAs	DAP ($mGycm^2$)
70	10	10.8	108	218 (Non-stitched)
80	10	10.8	108	260 (Non-stitched)
70	10	32.4	324	653 (Stitched)

Comments: The stitched method would produce DAP dose 3 times of non-stitched methods at the same kVp and mAs.

VITAE

Name	Miss Preeyaporn Srimawong
Date of birth	February 14, 1981
Place of birth	Saraburi, Thailand
Education	Faculty of Dentistry, Mahidol University D.D.S., 2005
	Faculty of Dentistry, Mahidol University Grad.Dip.in Clin.Sc. (Oral and Maxillofacial Radiology), 2007

Academic Publications

1. Preeyaporn Srimawong. Cone beam computed tomography in dentistry. J Dent Assoc Thai 2008;58:26-38.
2. Srimawong P, Songkampol K, Fuangtharnthip P, Wongsirichat N. Application of cone beam computed tomography for supernumerary tooth. Mahidol Dental Journal 2010;30:129-139.
3. Songkampol K, Srimawong P, Chidchuangchai W. Multiple Anomalies in Dental Tooth Shape: Lobodontia and Multiple Dens Invaginatus: A Case Report. J Dent Assoc Thai 2011;61.

Current work position and office

Lecturer at Department of Oral & Maxillofacial Radiology, Faculty of Dentistry, Mahidol University 6 Yoti Road, Phayatai, Ratchatewi, Bangkok 10400